# Listeriolysin S: A bacteriocin from Listeria monocytogenes that induces membrane permeabilization in a contact-dependent manner

Jazmín Meza-Torres, Mickaël Lelek, Juan Quereda, Martin Sachse, Giulia Manina, Dmitry Ershov, Jean-Yves Tinevez, Lilliana Radoshevich, Claire Maudet, Thibault Chaze, et al.

HAL Id: hal-03620714

https://hal.science/hal-03620714

Submitted on 12 May 2022

# Listeriolysin S: A bacteriocin from *Listeria monocytogenes* that induces membrane permeabilization in a contact-dependent manner

Jazmín Meza-Torres[a,b,c], Mickaël Lelek[d], Juan J. Quereda[e], Martin Sachse[f], Giulia Manina[g], Dmitry Ershov[h,i], Jean-Yves Tinevez[h], Lilliana Radoshevich[j], Claire Maudet[k], Thibault Chaze[l], Quentin Giai Gianetto[l,m], Mariette Matondo[l], Marc Lecuit[c,k,n], Isabelle Martin-Verstraete[o], Christophe Zimmer[d], Hélène Bierne[p], Olivier Dussurget[a,c], Pascale Cossart[b], and Javier Pizarro-Cerdá[a,1]

[a]Yersinia Research Unit, Microbiology Department, Institut Pasteur, 75015 Paris, France; [b]Bacteria-Cell Interactions Unit, Cell Biology and Infection Department, Institut Pasteur, 75015 Paris, France; [c]Université de Paris, Sorbonne Paris Cité, 75005 Paris, France; [d]Imaging and Modeling, Department of Computational Biology, Institut Pasteur, Centre National de la Recherche Scientifique, Unité Mixte de Recherche 3691, 75015 Paris, France; [e]Departamento Producción y Sanidad Animal, Salud Pública Veterinaria y Ciencia y Tecnología de los Alimentos, Facultad de Veterinaria, Universidad Cardenal Herrera-CEU, CEU Universities, 46115 Valencia, Spain; [f]Ultrastructural BioImaging, Institut Pasteur, 75015 Paris, France; [g]Microbial Individuality and Infection Group, Cell Biology and Infection Department, Institut Pasteur, 75015 Paris, France; [h]Image Analysis Hub, C2RT, Institut Pasteur, 75015 Paris, France; [i]Bioinformatics and Biostatistics Hub, Department of Computational Biology, Institut Pasteur, Centre National de la Recherche Scientifique, Unité de Service et de Recherche 3756, 75015 Paris, France; [j]Department of Microbiology and Immunology, Carver College of Medicine, University of Iowa, Iowa City, IA 52242; [k]Biology of Infection Unit, Institut Pasteur, Institut National de la Santé et de la Recherche Médicale Unité 1117, 75015 Paris, France; [l]Proteomics Platform, Mass Spectrometry for Biology Unit, Institut Pasteur, Centre National de la Recherche Scientifique, Unité de Service et de Recherche 2000, 75015 Paris, France; [m]Bioinformatics and Biostatistics HUB, Computational Biology Department, Institut Pasteur, Centre National de la Recherche Scientifique, Unité de Service et de Recherche 3756, 75015 Paris, France; [n]Division of Infectious Diseases and Tropical Medicine, Necker-Enfants Malades University Hospital, Institut Imagine, Assistance Publique-Hôpitaux de Paris, 75004 Paris, France; [o]Laboratoire Pathogenèses des Bactéries Anaérobies, Institut Pasteur, Centre National de la Recherche Scientifique, Unité Mixte de Recherche 2001, Université de Paris, 75015 Paris, France; and [p]Epigenetics and Cellular Microbiology Laboratory, Université Paris-Saclay, Institut National de Recherche pour l'Agriculture, l'Alimentation et l'Environnement, AgroParisTech, 78352 Jouy-en-Josas, France

**Listeriolysin S (LLS) is a thiazole/oxazole–modified microcin (TOMM) produced by hypervirulent clones of *Listeria monocytogenes*. LLS targets specific gram-positive bacteria and modulates the host intestinal microbiota composition. To characterize the mechanism of LLS transfer to target bacteria and its bactericidal function, we first investigated its subcellular distribution in LLS-producer bacteria. Using subcellular fractionation assays, transmission electron microscopy, and single-molecule superresolution microscopy, we identified that LLS remains associated with the bacterial cell membrane and cytoplasm and is not secreted to the bacterial extracellular space. Only living LLS-producer bacteria (and not purified LLS-positive bacterial membranes) display bactericidal activity. Applying transwell coculture systems and microfluidic-coupled microscopy, we determined that LLS requires direct contact between LLS-producer and -target bacteria in order to display bactericidal activity, and thus behaves as a contact-dependent bacteriocin. Contact-dependent exposure to LLS leads to permeabilization/depolarization of the target bacterial cell membrane and adenosine triphosphate (ATP) release. Additionally, we show that lipoteichoic acids (LTAs) can interact with LLS and that LTA decorations influence bacterial susceptibility to LLS. Overall, our results suggest that LLS is a TOMM that displays a contact-dependent inhibition mechanism.**

Listeriolysin S (LLS) | bacteriocin | *Listeria monocytogenes* (*Lm*) | contact-dependent inhibition (CDI) | microfluidic microscopy

*L*isteria monocytogenes (*Lm*) is a gram-positive foodborne pathogen responsible for listeriosis, a disease characterized by meningitis in the newborn, bacteremia in immunocompromised or elderly individuals, and abortions in pregnant women (1, 2). To date, the most severe human listeriosis outbreaks have been associated with a subset of *Lm* lineage I strains (3, 4). These hypervirulent strains harbor a biosynthetic gene cluster that encodes for the small peptide Listeriolysin S (LLS) (3, 5). Though initially proposed to be a virulence factor via its hemolytic activity (3), it has since been shown that LLS is a weak hemolytic factor that does not display cytotoxic effects on eukaryotic cells, does not induce specific immune cell responses, and has no impact on cellular infection by *Lm* (6). Instead, LLS is a bacteriocin that

targets several gram-positive bacterial species in vitro including *Lactococcus lactis* as well as hypovirulent *Lm* strains, and promotes intestinal colonization by *Lm* in vivo through modulation of the host gut microbiota composition (7, 8).

Biosynthetic gene clusters similar to the LLS operon (shown in *SI Appendix*, Fig. S1A) are widely conserved in different bacterial phyla (9). They encode for 1) a prepeptide (unmodified peptide) (*SI Appendix*, Fig. S1B), 2) an ATP-binding cassette transporter (ABC transporter) that exports the toxin once it is posttranslationally modified, 3) an immunity protein, and 4) an enzymatic complex

### Significance

*Listeria monocytogenes* (*Lm*) is a bacterial pathogen that causes listeriosis, a foodborne disease characterized by gastroenteritis, meningitis, bacteremia, and abortions in pregnant women. The most severe human listeriosis outbreaks are associated with a subset of *Lm* hypervirulent clones that encode the bacteriocin Listeriolysin S (LLS), which modifies the gut microbiota and allows efficient *Lm* gut colonization and invasion of deeper organs. Our present work identifies the killing mechanism displayed by LLS to outcompete gut commensal bacteria, demonstrating that it induces membrane permeabilization and membrane depolarization of target bacteria. Moreover, we show that LLS is a thiazole/oxazole–modified microcin that displays a contact-dependent inhibition mechanism.

MICROBIOLOGY

that allows the posttranslational modification (PTM) of the toxin with thiazole, oxazole, and/or methyl-oxazole heterocycles (10). This family of thiazole/oxazole–modified microcins (TOMMs) includes microcin B17 (MccB17) from *Escherichia coli*, streptolysin S (SLS) from *Streptococcus pyogenes*, and plantazolicin (PZN) from *Bacillus methylotropicus* (10–12). MccB17 is an antimicrobial peptide that targets *E. coli* and acts as a DNA gyrase inhibitor (13), while PZN displays narrow activity against *Bacillus anthracis* through bacterial membrane depolarization and association with cardiolipin microdomains (11). In contrast, SLS is a major cytotoxic and hemolytic virulence factor produced by group A *S. pyogenes* (14, 15), which targets erythrocytes, leukocytes, platelets, and subcellular organelles, and can display lytic activity against bacterial protoplasts (16–19).

We have previously shown that LLS kills specific gram-positive bacteria (7) but its mechanism of action remains unknown. In the present study, we demonstrate that LLS remains localized to the bacterial cell membrane of LLS-producer bacteria and exerts its killing mechanism via direct contact between LLS-producer and -target bacteria, impairing membrane integrity of target bacteria and inducing membrane depolarization. Our previous findings identified a key role for LLS in the modulation of the host microbiota by *Lm* hypervirulent strains. Our present work suggests that hypervirulent *Lm* may outcompete bacteria by means of LLS in a contact-dependent manner.

## Results

### LLS Is Associated with the Cell Membrane of LLS-Producer Bacteria.

We have previously demonstrated that LLS is not expressed in vitro, and that its production is detected only in vivo within the intestine of infected animals (7). To identify in vitro conditions that mimic the intestinal environment leading to LLS expression, we performed a screen exposing the *Lm* F2365 strain to libraries of molecules that mimic or are homologous to components present in the gastrointestinal tract, and we monitored LLS expression using a green fluorescent protein (GFP) reporter. We also performed cocultures of *Lm* F2365 with previously identified target bacterial species to explore whether target bacteria could be the LLS-activating signal. We did not find any molecule or condition that triggers LLS production in vitro. Therefore, to assess LLS activity, we introduced the constitutive promoter pHELP upstream of the LLS operon in the F2365 strain, a technique previously employed by Cotter and colleagues (3). The strain F2365:pHELP (designated as LLS$^+$) expresses all the genes of the LLS operon (*SI Appendix*, Fig. S1C). While there is a potential caveat associated with the constitutive expression of LLS, there was no detectable effect on growth nor were there any morphological changes in the LLS$^+$ strain as compared with the parental *Lm*.

Production of antibodies against the biologically functional LLS represents a challenge due to the putative PTMs of the mature LLS form and due to its small size (4.9 kDa including the leader peptide and 2.3 kDa without it). Therefore, to label LLS, we generated LLS-FLAG and -hemagglutinin (HA) constructs in the LLS$^+$ background strain (7). We confirmed that the LLS constructs were fully functional, since they retained bactericidal activity against target bacteria (*SI Appendix*, Fig. S2A) and displayed weak hemolytic activity comparable to that of the parental strain (*SI Appendix*, Fig. S2B). To study LLS distribution within bacteria and in the extracellular environment, we performed a fractionation experiment as previously described (20), leading to the separation of the bacterial cytoplasm, membrane, and cell wall as well as the supernatant. An LLS$^+$ strain without tags was used as a negative control (Fig. 1A and *SI Appendix*, Fig. S2C). Our results clearly demonstrate that in our growth conditions, LLS is detected only in the bacterial cell membrane and cytoplasm, and is neither secreted in the supernatant nor associated with the bacterial cell wall (Fig. 1 A and B). To determine
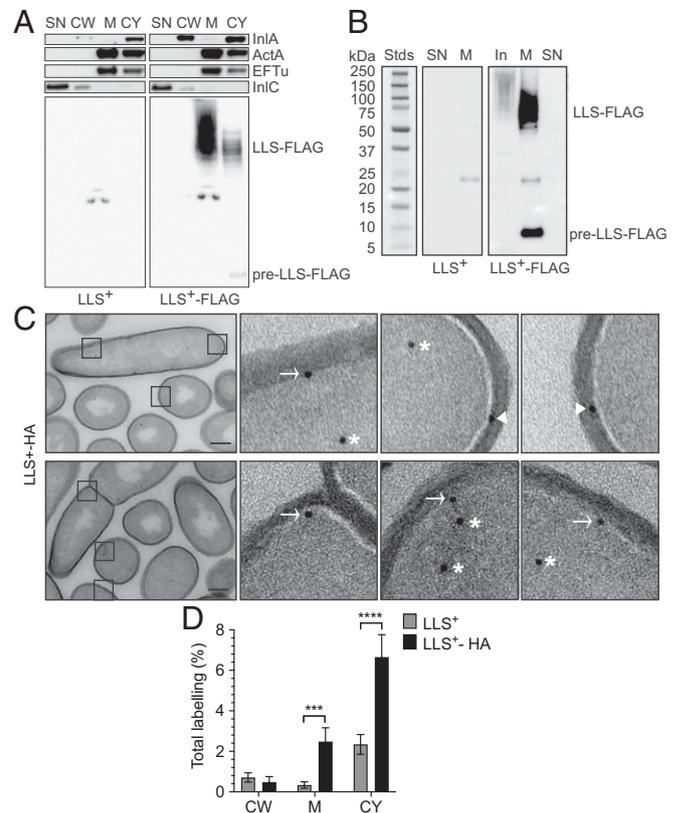


**Fig. 1.** LLS is not actively secreted and is located at the cell membrane. (*A*) Localization of LLS by fractionation experiments. Western blot analysis was performed on a strain expressing LLS$^+$ (negative control) and a strain expressing LLS$^+$-FLAG (FLAG at the C terminus). Proteins were fractionated into four compartments: supernatant (SN), cell wall (CW), membrane (M), and cytoplasm (CY). InlA, ActA, EF-Tu, and InlC were used as controls for fractionation. Equivalent amounts of each fraction, corresponding to 100 μL of bacterial culture, were separated by sodium dodecyl sulfate–polyacrylamide gel electrophoresis (SDS-PAGE) and submitted to immunodetection using the indicated antibodies. Data from one representative experiment out of the three performed are shown. Pre-LLS FLAG, unmodified LLS peptide. (*B*) LLS SN and M fractions were immunoprecipitated on a strain expressing LLS$^+$ (negative control) and a strain expressing LLS$^+$-FLAG by using magnetic beads coupled to anti-FLAG antibodies. Equivalent amounts of each fraction, corresponding to 2.5 mL of bacterial culture, were separated by SDS-PAGE and submitted to immunodetection using the anti-FLAG antibody. Input (In) was from the membrane fraction. Data from one representative experiment out of the three performed are shown. The prestained protein standards (Stds) are shown (*Left*) with the respective molecular mass in kDa. (*C*) Location of LLS by TEM. An anti-HA colloidal gold-coupled antibody was used to detect LLS on a strain expressing LLS$^+$-HA (HA at the C terminus). (*C, Insets*) Enlargement of areas of LLS detected at the internal side of the membrane (arrows) and external side of the membrane (arrowheads) and cytoplasm (asterisks). (Scale bars, 200 nm.) (*D*) Quantification of the total labeling (%) of LLS$^+$ (negative control) and LLS$^+$-HA in the CW, M, and CY compartments obtained from TEM shown in *C*. Positive signals in the M and CY of the LLS$^+$-HA sample are significantly different from background noise present in the LLS$^+$ sample. Error bars show SEM. Multiple *t* tests were performed to compare different compartments. M: ***$P = 0.000143$; CY: ****$P = 0.000069$. LLS$^+$ $n = 106$; LLS$^+$-HA $n = 59$.

whether absence of LLS detection in the supernatant is due to its very low abundance, we performed an immunoprecipitation assay to concentrate the supernatant of the LLS$^+$-FLAG strain. These data confirm the total absence of LLS in the supernatant and its presence in the membrane and cytoplasmic fraction (Fig. 1B). In the cytoplasm, we detect a band of ∼6 kDa corresponding to the expected molecular mass of a monomeric tagged LLS prepeptide, but we also detect a higher–molecular mass

smear (between 50 and 250 kDa) which we hypothesize to be the LLS posttranslational heterocyclic molecule (Fig. 1A). This smear is observed using both the LLS⁺-FLAG and -HA constructs (Fig. 1A and *SI Appendix*, Fig. S2C), suggesting that it is specific for the LLS structure. Since our fractionation protocol involves bacterial overnight incubation with mutanolysin, to exclude the possibility that the observed smear is a product of LLS degradation, we lysed bacteria without fractionation and without overnight incubation. We confirmed the presence of the LLS smear using this milder preparation (*SI Appendix*, Fig. S2D).

To investigate whether the high–molecular mass smear corresponds to the LLS posttranslational heterocyclic molecule, we performed a bacterial subcellular fractionation assay with the tagged and nontagged LLS⁺ strains upon deletion of the *llsB* gene, which encodes a putative subunit of the LLS posttranslational machinery (3) and is required for the biological activity of LLS (6). The high–molecular mass smear is indeed absent in the LLS⁺-FLAGΔ*llsB* strain (*SI Appendix*, Fig. S3A), suggesting that it corresponds to an LLS molecule that has been posttranslationally modified. Interestingly, the 6-kDa band corresponding to the monomeric tagged LLS prepeptide also disappears in the LLS⁺-FLAGΔ*llsB* strain (*SI Appendix*, Fig. S3A). To determine whether deletion of the *llsB* gene leads to polar effects, we performed a qRTPCR of the LLS operon genes in the tagged and nontagged LLS⁺ strains. The deletion of the *llsB* gene did not cause expression defects on the upstream or downstream genes of the operon (*SI Appendix*, Fig. S3B), suggesting that the *llsA* gene is normally transcribed but, in the absence of functional posttranslational machinery, the LLS prepeptide could be unstable. To verify whether LLS PTM occurs in the cytosol prior to export, we intended to block LLS export by deleting the LLS leader peptide (*SI Appendix*, Fig. S1B) or by mutating specific motifs present in the LLS leader peptide that have been proved to be essential for substrate recognition by the PTM complex (21). However, mutants of the LLS leader peptide were not viable in the LLS⁺ strain. We therefore attempted to block LLS export by mutating the putative ABC-like transporter system encoded by the *llsGH* genes present in the *lls* gene cluster (*SI Appendix*, Fig. S1A). Interestingly, a double-Δ*llsGH* mutant is viable in an F2365 wild-type background in which LLS is not produced but the mutant is not viable in an LLS⁺ *Lm* strain that constitutively expresses LLS. The failure to obtain these mutants suggests that once LLS is produced, it must be translocated through the membrane in order to avoid intoxication of producer cells.

We then analyzed the LLS subcellular location with imaging approaches. While an immunofluorescence assay failed in detecting LLS⁺-HA at the bacterial surface, quantitative immunogold transmission electron microscopy (TEM) confirmed that LLS⁺-HA is detected in both the cytoplasm and at the membrane of producer bacteria (Fig. 1 C and D). Moreover, a set of LLS-associated gold particles appeared to localize on the outer side of the membrane (Fig. 1C), suggesting that LLS could be exposed on the bacterial surface. To examine the localization of fluorescently tagged LLS at high spatial resolution, we turned to dual-color superresolution with two single-molecule localization microscopy methods: We used transiently binding Nile red dyes (22) to image the cell membrane with PAINT (23), and AF647 dyes coupled to anti–HA tag antibodies to image LLS⁺-HA by dSTORM (24). While LLS⁺-HA cannot be detected at the surface of intact bacteria (*SI Appendix*, Fig. S4), when the cell wall is digested with mutanolysin LLS⁺-HA is visible as discrete clusters of localizations on the exposed bacterial cell membrane (Fig. 2A). We analyzed the images to quantify the number of LLS clusters per bacterium and their location relative to the cell membrane (Fig. 2 B–D). In negative control bacteria (nontagged LLS⁺ *Lm*), we detected only 4 nonspecific clusters in the vicinity of 197 analyzed cells (2%), whereas in LLS⁺-HA *Lm*, we detected 119 LLS clusters for 357 analyzed bacteria (33%). While 71% of cells have

no detected LLS clusters, we counted one, two, or three clusters in 22, 5, and 1% of bacteria (Fig. 2D). We further calculated the distance of each LLS cluster to the membrane, as determined by fitting an ellipse to the Nile red localizations (Fig. 2B), and obtained an average distance of 3 nm, much smaller than the PAINT/dSTORM resolution, consistent with a localization of LLS clusters at the membrane of producer bacteria (Fig. 2C). Overall, our results indicate that LLS is not actively secreted to the bacterial extracellular space but rather primarily localized to the membrane of LLS-producer bacteria (Fig. 2C).

**Cell-to-Cell Contact between LLS-Producer and -Target Bacteria Favors LLS Bactericidal Activity.** To understand the mechanism of LLS transfer between LLS-producer and -target bacteria, we first assessed the potential bactericidal activity of LLS⁺ fractions on *L. lactis*, which we previously demonstrated to be LLS-sensitive (7). We incubated *L. lactis* for 24 h with supernatant, cell-wall, membrane, and cytoplasmic fractions isolated from LLS⁺ *Lm*. However, none of these fractions displayed bactericidal activity on *L. lactis* (Fig. 3A), suggesting that active bacterial metabolism is required for LLS activity. In agreement with this, exposure of *L. lactis* to LLS⁺ *Lm* inactivated by different methods (boiling, antibiotic treatment, or ultraviolet [UV] light exposure) prevented *L. lactis* killing (Fig. 3A).

Since our results demonstrate that LLS is not released to the bacterial extracellular environment, we suspected that LLS activity might be dependent on proximity or direct contact between LLS-producer and -target bacteria. To evaluate whether LLS activity requires bacterial cell-to-cell contact, LLS⁺ *Lm* and *L. lactis* were cocultivated using a transwell system in which bacteria are separated by a porous membrane (Fig. 3B). We compared two different transwell systems with different membrane pore sizes: 0.4 and 8 μm. The 0.4-μm membrane allows the diffusion of media and molecules secreted by the bacteria, while the 8-μm membrane allows bacterial passage through the pore and thus direct contact of whole bacteria. Interestingly, we solely observed the bactericidal effect of LLS when using the 8-μm membrane system (Fig. 3B), suggesting that direct contact between LLS-producer and -target bacteria favors LLS bactericidal activity. Indeed, this activity was absent using the 0.4-μm system, or when target bacteria were incubated with the negative control strain LLS⁻ (Δ*llsA*) (Fig. 3B), arguing against the alternative hypothesis that reduction of *L. lactis* numbers could be due instead to dilution of target bacteria through the 8-μm porous membrane.

In the above experiments, we cannot exclude the possibility that LLS could form high–molecular mass aggregates that do not cross the 0.4-μm membranes. To rule out this possibility and to further characterize the LLS killing effect on target bacteria, we performed single-cell time-lapse microscopy employing a microfluidic culture system (25) (Fig. 4A) in which we cocultured the target *Lm* 10403S strain constitutively expressing GFP (26) together with LLS⁺ (or the negative control LLS⁻) *Lm* constitutively expressing the tdTomato reporter. We used 10403S bacteria as a target because the antagonistic effect of LLS was previously assessed in in vitro cocultures using this hypovirulent *Lm* strain (7), and also because the F2365 and 10403S cells have similar growth rates (*SI Appendix*, Fig. S5). Interestingly, an increase in the GFP fluorescence was detected in the contact points between the producer (LLS⁺-tdTomato) and the target (10403S-GFP) bacteria but not between the Δ*llsA* (LLS⁻ tdTomato) and the target bacteria (Fig. 4 B and C). Furthermore, we observed that only when the target bacteria encounter the producer LLS⁺ strain (and not the LLS⁻) do the producer bacteria dominate over time (Fig. 4D).

We hypothesized that the increase in the GFP fluorescence in the target bacteria could be attributed to the accumulation of the GFP inside cells, due to a halted bacterial growth. To investigate this hypothesis, the 10403S-GFP growth rate and doubling time were measured from image sequences. Our results confirm that
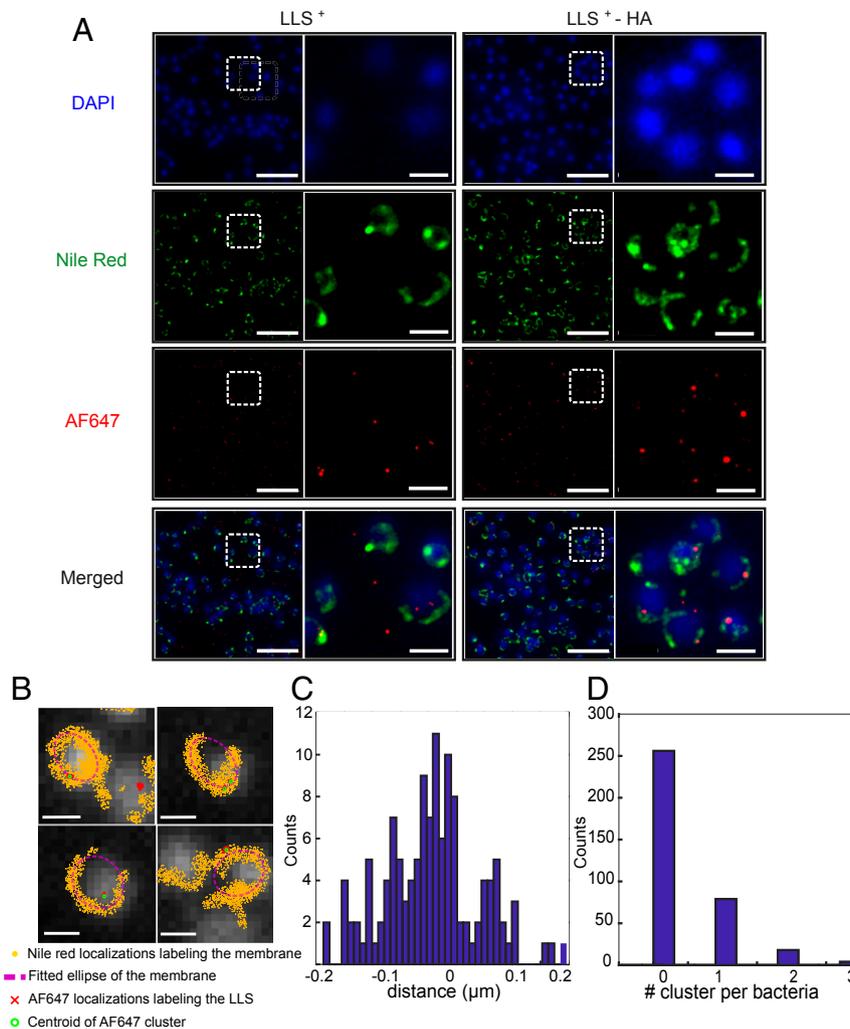
Meza-Torres et al.
Listeriolysin S: A bacteriocin from *Listeria monocytogenes* that induces membrane permeabilization in a contact-dependent manner

PNAS | 3 of 11
https://doi.org/10.1073/pnas.2108155118

**Fig. 2.** Superresolution imaging of LLS⁺-HA distribution at the cell membrane. Dual-color superresolution PAINT/dSTORM microscopy was performed on a strain expressing LLS⁺ (negative control; *Left*) and a strain expressing LLS⁺-HA (*Right*). (*A*) Protoplasts were fixed and imaged in the DAPI channel (blue). The bacterial membrane was imaged using PAINT with Nile red dye (green). LLS was imaged using dSTORM microscopy with an AF647-conjugated anti-HA monoclonal antibody (red). The images show a large field of view (scale bars, 5 μm) and a magnified view of the dashed white box (scale bars, 1 μm). (*B*) Ellipses are fitted to Nile red localizations to outline the membrane of manually selected cells. LLS clusters and their centroids were determined from A647 localizations. (Scale bars, 500 nm.) (*C*) Distribution of signed Euclidian distances between AF647 clusters and ellipses (clusters inside the ellipse have negative distances; clusters outside have positive distances). Mean signed distance is 3 nm. (*D*) Distribution of the number of LLS clusters per cell: 71% of cells have no LLS cluster; 22, 5, and 1% of bacteria have 1, 2, and 3 LLS clusters, respectively. Data are from $n = 357$ cells in three fields of view.

the bacterial growth is arrested for target cells that are in direct contact with the LLS⁺ bacteria (Fig. 5*A*). This is not observed when target bacteria are physically distant from producer cells, or when they are in contact with LLS⁻ (Δ*llsA*) bacteria (Fig. 5*A*), demonstrating that the growth arrest of target cells is dependent upon direct contact with bacteria producing LLS. Indeed, the $k$ constant for target cells in direct contact with the LLS⁺ strain was 0.0097 min⁻¹, with an average doubling time of 110 min. In contrast, the $k$ constant of target cells, either not in contact with producer cells or in contact with LLS⁻, was 0.02 min⁻¹, with an average doubling time of 40 min, which is expected for rich media–grown *Lm*.

Remarkably, LLS-target cells that had more than one LLS⁺-producer cell surrounding them were more likely to have their growth arrested and to die (Fig. 5*B*). We also found that LLS-target cells in contact with LLS⁺-producer cells are unable to divide, and shrink before experiencing lysis (Fig. 5*C*). Together, our results indicate that the LLS can exert a contact- and concentration-dependent growth inhibition mechanism on target cells impeding their cell division.

**LLS Induces Cell-Membrane Permeabilization Exclusively of Target Cells that Are in Direct Contact with LLS-Producer Bacteria.** To identify the molecular mechanisms underlying the LLS contact-dependent bactericidal activity, we investigated whether LLS could impair peptidoglycan or cell-membrane integrity. To investigate a potential impact of LLS on peptidoglycan, we performed click chemistry followed by flow cytometry analysis. Briefly, target cells (*L. lactis*) were incubated overnight with 3-azido-D-alanine (ADA) to allow its incorporation into the peptidoglycan and then target bacteria were washed and cocultivated with LLS⁻ or LLS⁺ *Lm*. Afterward, target bacteria were labeled by click-chemistry reaction (reactive with ADA) to analyze the fluorescence intensity of target cells by flow cytometry. The fluorescence intensity of labeled target cells is proportional to the ADA incorporated into the peptidoglycan. The fluorescence intensity levels of target bacteria incubated with LLS⁻ or LLS⁺ were equivalent (*SI Appendix*, Fig. S6), suggesting that the peptidoglycan structure was intact and that LLS does not affect the integrity of peptidoglycan.
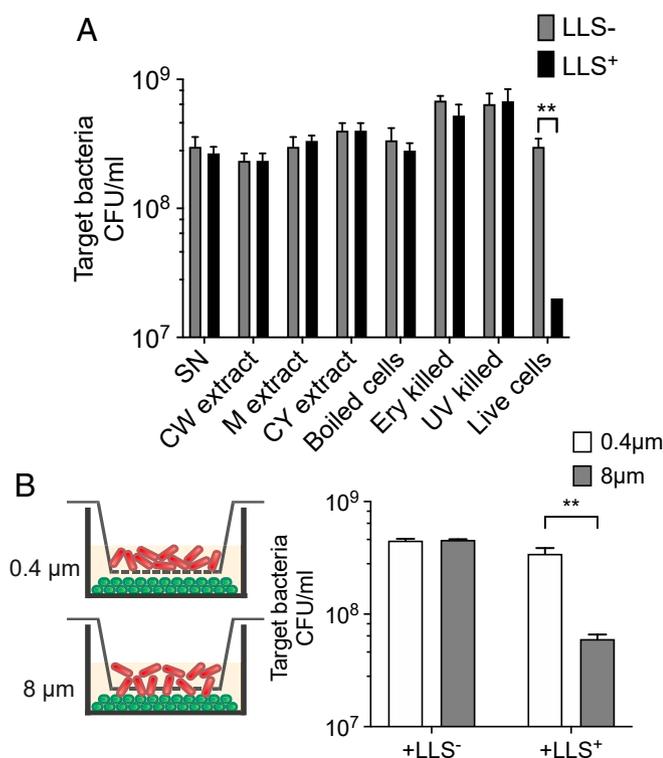
**Fig. 3.** LLS bactericidal activity requires cell–cell contact between a producer and target bacteria. (*A*) Survival of target bacteria when cocultured with *Lm* fractions with erythromycin (Ery) or UV light–killed bacteria, and with live *Lm*. Target bacteria were incubated for 24 h in BHI with LLS-producer bacteria (LLS⁺) or LLS mutant bacteria (LLS⁻) live cells or fractions, or inactivated bacteria. CFU, colony-forming unit. (*B*) A coculture was performed using the split-well setup shown (*Left*). The membrane separating the producer bacteria (LLS⁺ or LLS⁻) from the target bacteria had a pore size of 8 or 0.4 μm. Data from one representative experiment out of the three performed are shown. Error bars show SEM. Multiple two-tailed unpaired *t* tests were performed. **$P = 0.004066$ (*A*), **$P = 0.002921$ (*B*); $n = 3$.

To investigate whether LLS could modify cell-membrane permeabilization, we carried out time-lapse microfluidic microscopy and added SYTOX blue dye, which exclusively penetrates and stains cells that have lost their membrane integrity (27). Since brain heart infusion (BHI) quenches the SYTOX signal, after the first 3 h of cell growth in BHI medium, we performed the perfusion of SYTOX with phosphate-buffered saline (PBS), which stopped bacterial growth due to the lack of nutrients. Using this setup, we found that SYTOX exclusively stains 10403S target cells that are in direct contact with LLS⁺ bacteria, whereas 10403S target cells that are not in contact with LLS producers remain unstained (Fig. 6 *A* and *B*). Interestingly, once the producer and the target bacteria are in intimate contact, the LLS permeabilization effect is not immediate and requires an incubation period from 1 to 2 h after the addition of the SYTOX dye (Fig. 6*B*). This is consistent with the timing of GFP accumulation in target cells that are in direct contact with LLS-producer cells (Fig. 4 *B* and *C*), where the bactericidal effect also takes place from 1 to 2 h after the contact. As observed in Fig. 4*C*, the activity of LLS is lost over time, probably due to the lack of nutrients upon SYTOX/PBS perfusion. When performing a recovery assay by perfusing BHI and SYTOX a second time, bacteria restart growing and LLS resumes its activity (*SI Appendix*, Fig. S7). This assay confirms that LLS activity requires actively growing bacteria and suggests that LLS requires an energy-dependent transport mechanism. These results are consistent with our previous observations showing that

inactivated producer cells display no LLS-associated bactericidal activity (Fig. 3*A*).

The increase in cell-membrane permeability is a sign of membrane damage and/or pore formation that could lead to the release of small molecules such as adenosine triphosphate (ATP) (28). We decided therefore to measure the release of ATP into the supernatant of *L. lactis* cocultivated with LLS⁻ or LLS⁺ *Lm*. We detected an increase in the ATP levels released into the supernatant of *L. lactis* cells cocultivated with LLS⁺ *Lm* compared with the ATP levels of *L. lactis* cocultivated with LLS⁻ *Lm* (*SI Appendix*, Fig. S8). This result therefore supports our hypothesis that LLS causes cell-membrane permeabilization of target bacteria. Taken together, these results demonstrate that LLS prevents target cell division and growth in a contact-dependent manner, leading to cell-membrane permeabilization and small-molecule leakage.

**LLS Induces Target Cell-Membrane Depolarization.** The efflux of ions or small molecules such as ATP as a consequence of cell-membrane permeabilization leads to the dissipation of the proton motive force by altering the transmembrane potential and pH gradient, leading to cell death (28). To directly assess the LLS impact on the membrane potential of target cells, membrane depolarization assays were performed (Fig. 7*A*). We used the voltage-dependent dye DiBAC₄(3) that upon cell depolarization can enter cells and stain the cellular membranes (29). *L. lactis* was cocultivated with LLS⁺- or LLS⁻-tdTomato *Lm* and DiBAC₄(3) was added followed by fluorescence quantification. As a positive control, we used the bacteriocin nisin that induces cell-membrane depolarization of our *L. lactis* that lacks the nisin operon (Fig. 7*A*). Upon coculture with LLS⁺ cells, around 20% of target *L. lactis* displayed an increase in DiBAC₄(3) fluorescence, whereas *L. lactis* cocultured with LLS⁻ cells or cultured alone did not (Fig. 7 *B* and *C*). The percentage of target depolarized cells increased after 4 and 6 h of cocultures with producer cells (around 40 and 70%, respectively) (Fig. 7*B*). Also, the DiBAC₄(3) fluorescence increased over time when target cells were exposed to producer cells (Fig. 7*C*). We conclude therefore that LLS is able to induce membrane depolarization in target cells.

**Exposure to LLS Promotes Noncanonical ATP Production in Target Cells.** To further characterize the mechanism of action of LLS, we performed mass spectrometry–based proteomics of 10403S target bacteria cocultivated with LLS⁺ or with LLS⁻ *Lm*. Near 1,000 proteins (approximately half of the *Lm* proteome) were identified in our analysis. When comparing target bacteria cocultivated with LLS⁺ and with LLS⁻, 13 proteins were significantly up-regulated and 2 unknown proteins were down-regulated in target cells (*SI Appendix*, Fig. S9*A* and Table S4). Additionally, 18 proteins were exclusively present in target cells in the presence of LLS⁺ bacteria (*SI Appendix*, Table S4), while 28 proteins were exclusively present in target cells in the presence of LLS⁻ bacteria (*SI Appendix*, Table S5).

Remarkably, exposure to LLS leads to a metabolic switch in target cells that favors production of ATP, minimizing simultaneously ATP consumption (*SI Appendix*, Fig. S9*B*). For example, in the presence of LLS⁺ *Lm*, target 10403S bacteria overproduce pyruvate oxidase, butyryl transferase, and butyrate kinase, which are enzymes that support ATP production at the substrate level (*SI Appendix*, Fig. S9*B*) under conditions of membrane depolarization (30). The methyl-glyoxal shunt enzymes are also favored in the presence of LLS, restoring inorganic phosphate levels (necessary for ATP production) under conditions of phosphate limitation (31) (*SI Appendix*, Fig. S9*B*). The production of ATP precursors was additionally favored through induction of 1) the noncanonical nucleoside triphosphate pyrophosphatase RdgB, which produces guanosine monophosphate and adenosine monophosphate precursors from inosine triphosphate and xanthosine 5′-triphosphate
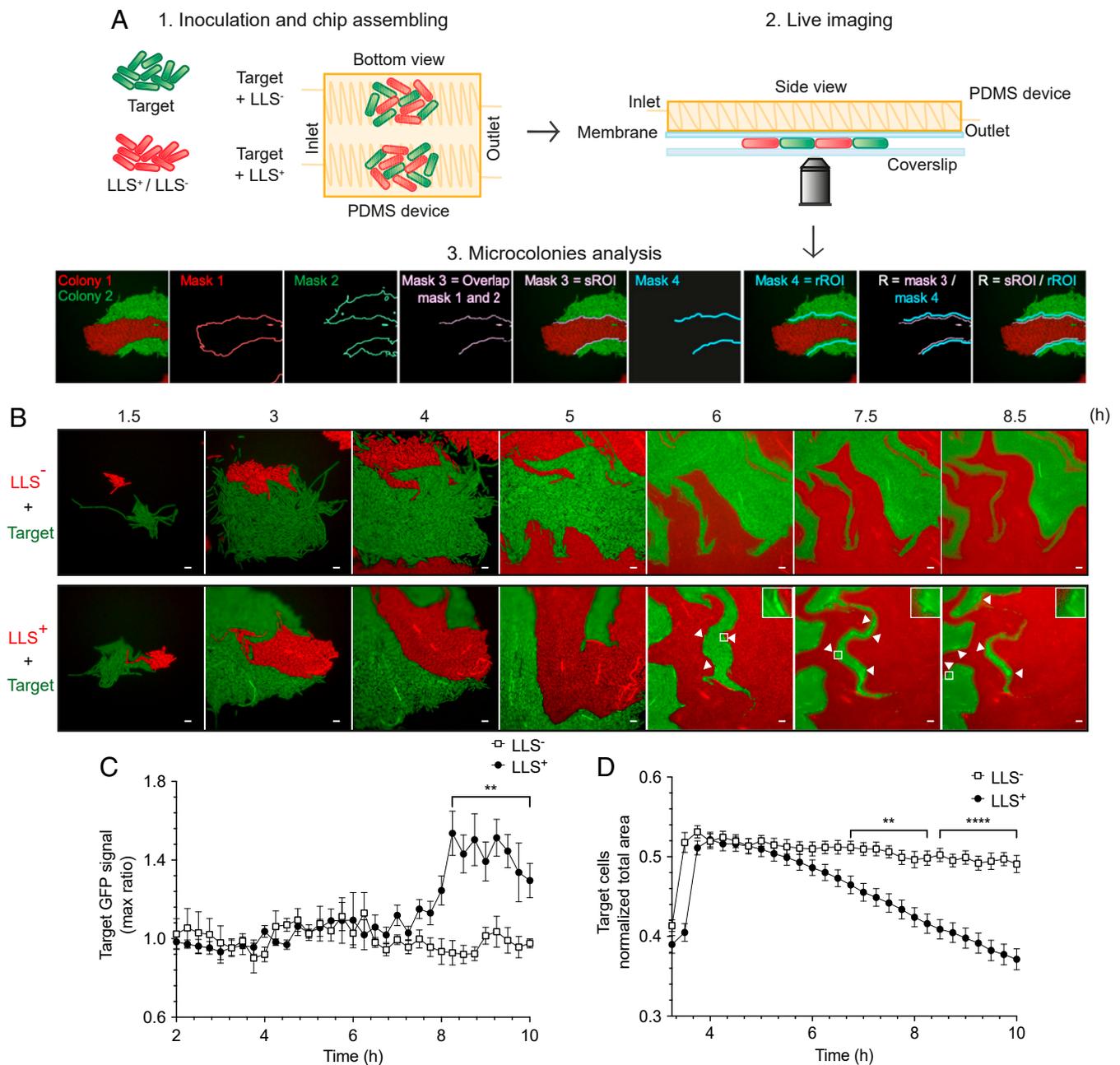
Meza-Torres et al.
Listeriolysin S: A bacteriocin from *Listeria monocytogenes* that induces membrane permeabilization in a contact-dependent manner

PNAS | 5 of 11
https://doi.org/10.1073/pnas.2108155118

**Fig. 4.** LLS inhibits the growth of target cells over time. (*A*) Schematic representation of microfluidics experiments. Top and side views of the assembled microfluidic device used for single-cell time-lapse microscopy (1). *Lm* LLS-producer bacteria (LLS⁺) and *Lm* LLS mutant bacteria (LLS⁻) express tdTomato constitutively and *Lm* target bacteria express GFP constitutively from an integrative plasmid (2). Bacteria are trapped between the coverslip and a semi-permeable membrane, fed by diffusion of medium, and imaged every 15 min during 10 h (3). Microcolonies of the target and producer bacteria are segmented (mask 1 and mask 2) to obtain the intersection between them (mask 3) which is the signal region of interest (sROI). The reference ROI (ROI, mask 4) includes the target bacteria not in contact with LLS⁺ or LLS⁻ bacteria. The ratio (*R*) between the ROIs (*R* = sROI/rROI) was analyzed over time. (*B*) Time-lapse microscopy snapshots of LLS⁺ or LLS⁻ (tdTomato) and target bacteria (GFP) over time. Data from one representative experiment out of the two performed are shown. (*B, Insets*) Enlargement of areas of LLS⁺ in contact with target bacteria; arrowheads show areas where the GFP fluorescence increased. (Scale bars, 3 0μm.) (*C*) Quantification of green fluorescence intensity of target bacteria in contact with LLS⁺ or LLS⁻ bacteria obtained from *R* (shown in *A*) represented as max ratio. Multiple unpaired *t* tests with Holm–Sidak correction were performed. *P* values are significant from 8 h, 15 min (**$P < 0.01$); LLS⁻ $n = 7$; LLS⁺ $n = 13$. (*D*) Quantification of the target cell total area over time. The area is normalized according to the area occupied by LLS⁺ or LLS⁻ bacteria. The area is represented as a percentage of the snapshot total area. Multiple unpaired *t* tests with Holm–Sidak correction were performed. *P* values are significant from 6 h, 45 min (**$P < 0.01$) and from 8 h, 30 min (****$P < 0.0001$); LLS⁻ $n = 26$; LLS⁺ $n = 33$. Error bars show SEM.

(*SI Appendix*, Fig. S9B) (32), 2) an adenosine diphosphate (ADP) ribose pyrophosphatase, allowing the deconjugation of ADP sugars (33), and 3) the nucleotide exchange factor GrpE, able to dissociate ADP from the nucleotide-binding DNaK cleft (34). Reduction of ATP consumption is exemplified by the overproduction of the dihydroxyacetone kinase DhaL, which uses a phosphoprotein instead of ATP as a phosphoryl donor (35). Altogether, these results show that in the presence of LLS, target cells adapt their metabolism to phosphate limitation and counteract the ATP efflux and loss of membrane potential.
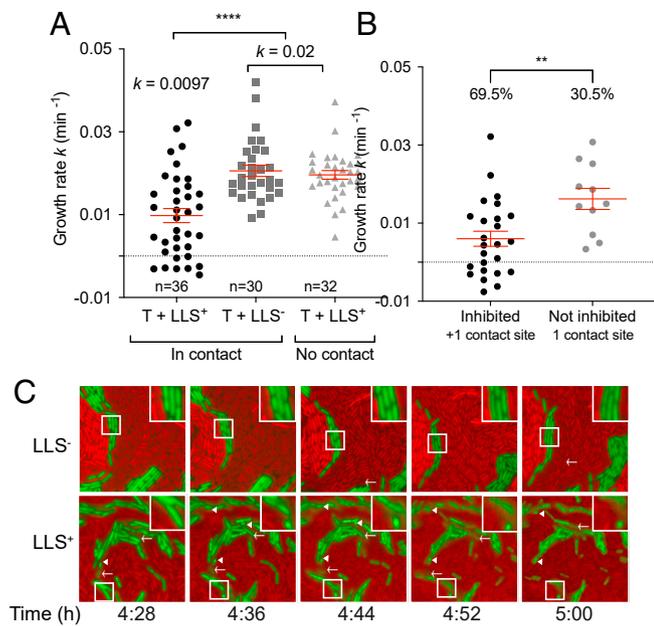
**Fig. 5.** LLS arrests the cell division of target cells in a contact-dependent manner. (A) Growth rate of target bacteria in contact or not with LLS$^+$ bacteria or in contact with LLS$^-$ bacteria represented in min$^{-1}$ ($k$ constant). (B) Growth rate of target bacteria in contact with one LLS$^+$ bacterium (one contact site) or more LLS$^+$ bacteria (more than one contact site) represented in min$^{-1}$ ($k$ constant). The bacteria in contact with one LLS$^+$ bacterium represent 30.5% of the population and do not die. The bacteria in contact with more LLS$^+$ bacteria represent 69.5% of the population and die. The bacterial growth rate ($k$ constant) was calculated by fitting an exponential curve to size measurements over the lifetime of the cells. Data from one representative experiment out of the two performed are shown. Error bars show SEM. Multiple two-tailed unpaired $t$ tests were performed. ****$P < 0.0001$ (A), **$P = 0.0053$ (B). (C) Representative time-lapse microscopy snapshots of LLS$^+$ or LLS$^-$ (tdTomato) and target bacteria (GFP) over time showing the shrinking (arrowheads and white squares) and lysis (arrows) of target cells in contact with LLS$^+$.

**LTA Can Interact with LLS and LTA Decorations Influence Bacterial Susceptibility to LLS.** We next investigated molecular determinants which could impact transfer and sensitivity to LLS. The membrane-bound TOMM SLS can be extracted from the membrane of *S. pyogenes* by carrier molecules, such as lipoteichoic acids (LTAs) (36, 37). Since our results show that LLS is also a membrane-bound molecule, we explored whether LLS interacts with purified LTA from *Staphylococcus aureus*, a bacterial species sensitive to the activity of LLS (7). As shown in *SI Appendix*, Fig. S10A, upon incubation of *Lm* with *S. aureus* LTA, only bacterial extracts from LLS$^+$ and LLS$^+$-FLAG cells (but not from LLS$^-$ cells) display a hemolytic phenotype associated with LLS activity (*SI Appendix*, Fig. S2B), suggesting that LTA is able to extract LLS from the *Lm* cell membrane (*SI Appendix*, Fig. S10A). When using the hemolytic extracts from LLS$^+$-FLAG cells to perform an immunoprecipitation, we detected a high–molecular mass smear similar to that of the LLS$^+$-FLAG present in cell-membrane fractions (*SI Appendix*, Fig. S10B). These results suggest that LTA is able to behave as a carrier molecule and can extract LLS from *Lm*. However, these extracts do not display bactericidal activity (*SI Appendix*, Fig. S11).

LTA is a molecule that can display diverse decorations that influence bacterial net surface charge as well as cell-wall density (38). To explore whether LTA decorations might impact susceptibility to LLS, we assessed the bactericidal activity of LLS on the LLS-sensitive *Lm* EGD strain (7), as well as on its isogenic *dltA* mutant, which cannot modify its LTA with D-alanine

decorations (39). In bacterial coculture experiments, both strains were found to be susceptible to LLS$^+$ *Lm*; however, the *dltA* mutant showed increased susceptibility to LLS compared with the wild-type EGD strain (*SI Appendix*, Fig. S12). Our results therefore suggest that LTA decorations influence the susceptibility of target bacteria to LLS.

## Discussion

Human listeriosis outbreaks are often caused by hypervirulent *Lm* lineage I strains characterized by the presence of the LLS biosynthetic cluster (3, 4), suggesting that LLS might be a critical determinant for listeriosis severity. LLS belongs to the TOMM family, which is present in pathogenic and nonpathogenic bacteria (9) with a diversity of functions such as cytotoxins (10, 21) or bacteriocins (7, 11, 12). The conservation and evolution of these biosynthetic clusters suggest that they present an advantage for the survival of pathogenic and symbiotic bacteria in very specific and different niches. In the case of *Lm*, we previously demonstrated that the presence of the LLS biosynthetic cluster represents an advantage in the gastrointestinal tract through modulation of the host microbiota composition, facilitating the colonization of the intestinal niche to allow further invasion of deeper tissues (7). In the present work, we explored the molecular mechanisms of action of LLS on target bacteria.

Furthermore, by employing subcellular fractionation assays, immunogold-labeling TEM, and superresolution microscopy, we demonstrate that LLS is primarily associated with the bacterial cell membrane and to a lesser extent with the cytoplasmic compartment of LLS-producer bacteria. An LLS high–molecular mass smear (present in the cytoplasm and at the cell membrane) is dependent on putative PTMs. The presence in the LLS operon of the genes *llsB/llsY/llsD*, which encode for a putative cyclodehydratase–dehydrogenase complex, suggests that LLS is posttranslationally modified with oxazole, thiazole, or methyloxazole heterocycles (10). Moreover, our previous results upon deletion of the *llsB* gene indicate that the LLS PTMs are critical for its biological activities (6). The LLS prepeptide displays 18 residues that can harbor PTMs (*SI Appendix*, Fig. S1B), putatively making LLS one of the most complex TOMMs. Despite our extensive efforts using mass spectrometry approaches, we have not been able to identify the structure of the mature, biologically active LLS. Solving the structure of the mature LLS will be critical to better understand not only its bactericidal mechanism of action but also its processing and transport from producer to target bacteria.

Our results indicate that LLS is not secreted in the culture medium of LLS-producer cells. However, LLS can be extracted from the bacterial membrane by yeast RNA core (3) or *S. aureus* LTA. Interestingly, while these fractions retain hemolytic activity, they do not display bactericidal activity. Similarly, purified bacterial membrane fractions containing LLS are nonbactericidal, and only metabolically active *Lm* display the capacity to kill target bacteria in a contact-dependent manner. Other cell-associated bacteriocins have been previously reported, including the bovicin HC5 from *Streptococcus bovis*, which can be extracted from the bacterial surface (40–42). However, these molecules do not display contact-dependent inhibition (CDI) mechanisms and their purification can be achieved without loss of bactericidal activity. At present, we ignore why LLS purified fractions or membranes are nonbactericidal. We speculate that the LLS structure is altered in these fractions, hampering recognition by receptors/carriers at the surface of target bacteria and/or inhibiting translocation to the target bacterial cell membrane, which has been identified in our work as a potential target compartment. We hypothesize therefore that the specific environment at the interphase between metabolically active LLS-producer bacteria and -target cells provides the conditions that allow transfer of a functional mature LLS molecule.
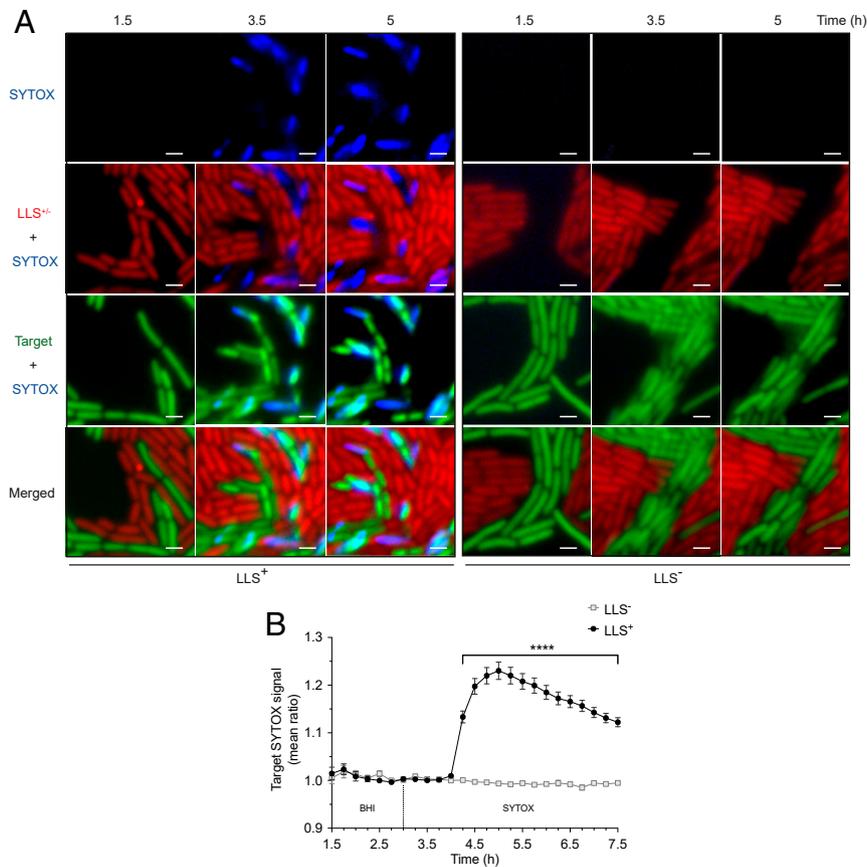
Meza-Torres et al.
Listeriolysin S: A bacteriocin from *Listeria monocytogenes* that induces membrane permeabilization in a contact-dependent manner

PNAS | 7 of 11
https://doi.org/10.1073/pnas.2108155118

**Fig. 6.** LLS induces cell-membrane permeabilization of the target bacteria that are in contact with LLS-producer bacteria. (*A*) Time-lapse microscopy enlarged snapshots of LLS⁺ or LLS⁻ and target bacteria over time. *Lm* LLS-producer bacteria (LLS⁺) and *Lm* LLS mutant bacteria (LLS⁻) express tdTomato constitutively and *Lm* target bacteria express GFP constitutively from an integrative plasmid. BHI medium was perfused for 3 h and then SYTOX blue dye was diluted in PBS and added after 2 h to label dying bacteria. (*B*) Quantification of SYTOX fluorescence intensity of target bacteria in contact with LLS⁺ or LLS⁻ bacteria obtained from *R* (shown in Fig. 3*A*) represented as mean of the SYTOX signal. Data from one representative experiment out of the two performed are shown. (Scale bars, 2 μm.) Error bars show SEM. Multiple unpaired *t* tests with Holm–Sidak correction were performed. *P* values are significant from 4 h, 15 min (****$P < 0.0001$); LLS⁻ $n = 26$; LLS⁺ $n = 32$.

From our study, LTA appears to be a bacterial surface determinant that contributes to susceptibility to LLS. The fact that purified LTA is able to extract LLS from the *Lm* membrane indicates that LTA can behave as a carrier for LLS. However, purified LTA-associated LLS is not bactericidal. These results open the way to the suggestion that upon intimate contact between LLS-producer and -target cells, LLS might use target bacterial LTA as a receptor/carrier for natural delivery. We also observed that changes in LTA decorations influence the biological activity of LLS, as absence of D-alanylations increases the susceptibility to the bacteriocin. The lack of D-alanine modification in the LTA leads to higher bacterial surface electronegativity (38), suggesting that net surface charges might influence LLS susceptibility, as it has been previously reported for antimicrobial peptides such as bacitracin, colistin, polymyxin B, nisin, and gallidermin (39). However, other pleiotropic effects of the Δ*dltA* mutation, including changes in cell-wall density, could also impact LLS susceptibility. The study of the potential role of LTA as a natural target of LLS deserves further investigation in future studies.

As mentioned, our microfluidic and microscopy experiments indicate that the contact-dependent (and also concentration-dependent) activity of LLS is initially associated with growth arrest of target bacteria (based on *k* constant measurements) and then leads to target membrane permeability and depolarization (based on fluorescent measurements of compartment-specific dyes). As opposed to other bacteriocins such as nisin (43), which alter peptidoglycan integrity and lead to bacterial explosion, our imaging experiments indicate that LLS-sensitive bacteria do not explode, as their signal gradually fades away as the bacterial content is emptied. This observation is congruent with our click-chemistry results indicating that LLS does not alter the peptidoglycan integrity, and also with our fluorescent and ATP measurements indicating that LLS alters target membrane permeability. Our proteomics results further suggest that the cell membrane may be the primary target of LLS activity, as target bacteria exposed to LLS display a metabolic switch to compensate for ATP leakage by increasing ATP production while minimizing ATP consumption. No other pathways such as peptidoglycan repair or DNA replication are modified in target bacteria upon LLS exposure. In this context, it is highly tempting to speculate that LLS might behave as a pore-forming bacteriocin.

Contrary to our observations concerning the LLS killing mechanism, previously studied TOMMs have not been reported to display CDI. Indeed, MccB17 (the prototypical TOMM) from *E. coli* is a secreted bacteriocin (12). SLS from *S. pyogenes* is also detected in bacterial supernatants (14, 15). For clostridiolysin S and plantazolicin from *Clostridium perfringens* and *B. methylotropicus*, respectively, the mechanism of transfer from producer to target bacteria has not been studied so far (11, 44). The only previously reported bacteriocin that displays a CDI mechanism is the two-peptide bacteriocin CdzC/CdzD from the gram-negative bacterium
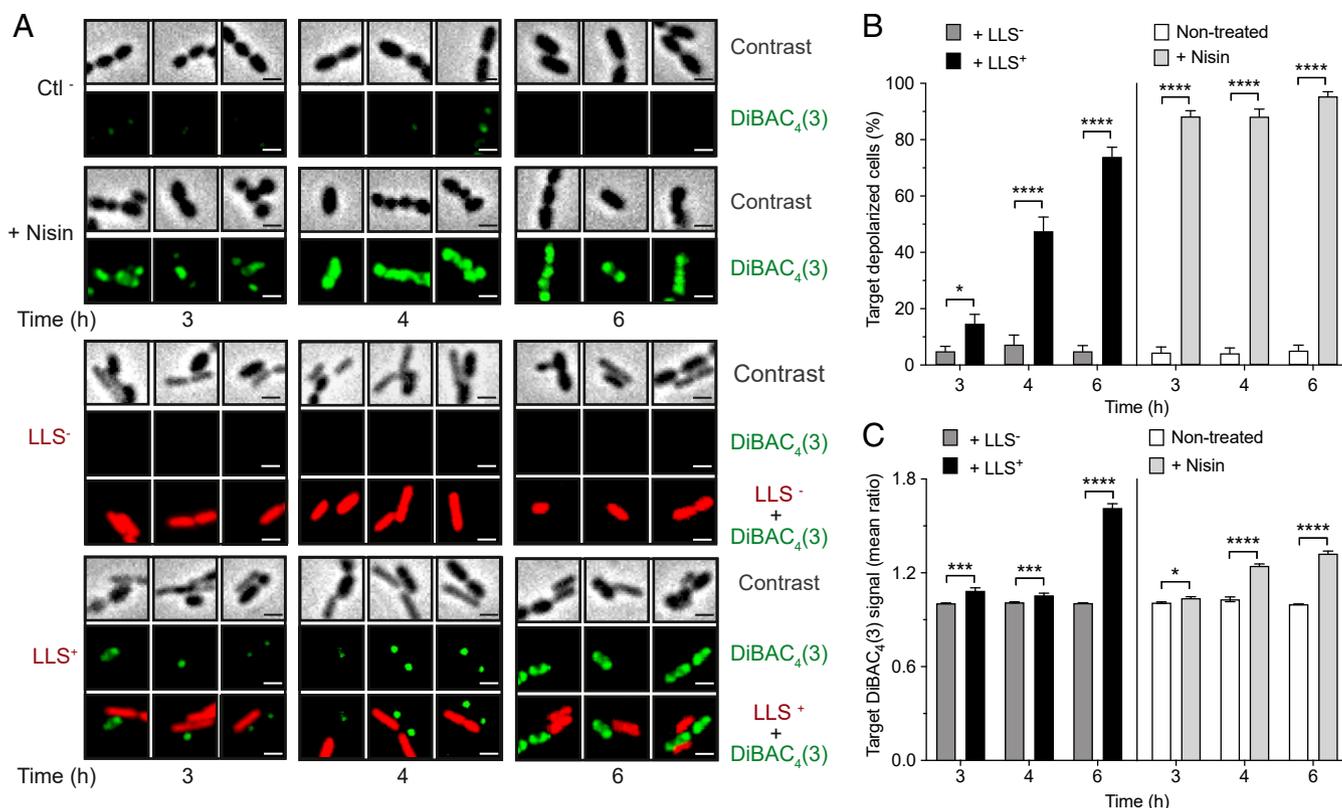
**Fig. 7.** LLS causes cell-membrane depolarization of target bacteria. (*A*) Three-dimensional reconstructed snapshots showing target bacteria (*L. lactis*) cultivated alone or with nisin (5 μM), and target bacteria cocultivated with LLS⁻ or LLS⁺ bacteria after different times of coculture. DiBAC₄(3) (2.5 μM) was added to BHI when bacteria were inoculated. (*B*) Percentages of depolarized target cells over time represent the % of target cells that yielded higher DiBAC₄(3) fluorescence intensity levels compared with target cells cultivated alone. (*C*) Quantification of DiBAC₄(3) fluorescence intensity of target bacteria is represented as a mean ratio (normalized to the background DiBAC₄[3] fluorescence levels). Data from one representative experiment out of three performed are shown. (Scale bars, 1 μm.) Error bars show SEM. Multiple unpaired *t* tests were performed. Significant *P* values are indicated by asterisks (*$P < 0.05$, ***$P < 0.001$, ****$P < 0.0001$).

*Caulobacter crescentus*, which forms insoluble aggregates that are retained on the outer membrane of producer cells (45). This bacteriocin, unrelated to TOMMs, uses a type I secretion system and an adhesion system encoded elsewhere in the genome, displaying a CDI mechanism against other gram-negative bacteria that lack the immunity protein CdzI (45). In gram-positive bacteria, CDI has been described for LXG domain proteins secreted by a type VII secretion system; however, these proteins can be detected in the bacterial supernatant, which is not the case for LLS (46).

The potential advantages of a CDI mechanism for LLS-producing bacteria are diverse. Within a complex environment such as the intestinal lumen in which hypervirulent *Lm* produce LLS to outcompete gut microbiota, the proximity between *Lm* and target bacteria can ensure effective killing and minimal LLS loss (45). As reported before, CDI systems could also limit non-producer "cheater" cells to benefit from secreted products (47). Alternatively, it could also be hypothesized that in vivo there are carrier molecules that allow the diffusion of LLS to distant locations. Testing this hypothesis should be the objective of future investigations. In any case, our present work identifies critical and unique features of the LLS bactericidal mechanism that open the way to better understand how this bacteriocin contributes to the hypervirulence of *Lm*.

## Materials and Methods

**Cocultures and Split-Well Coculture Bacterial Assays.** Coculture assays were performed for 24 h statically at 37 °C in microaerophilic conditions (6% $O_2$ and 5 to 10% $CO_2$) as previously described (7). Briefly, $5 \times 10^7$ bacteria from overnight (ON) cultures were inoculated into 5 mL of fresh BHI either alone or in coculture with another strain as indicated. At 24 h after inoculation, cultures were serially diluted and plated on BHI and Oxford agar plates (Oxoid). Experiments were performed three times independently.

For the split-well coculture assays, 6-well polystyrene plates were used with Millicell hanging inserts (PET membrane, 0.4- or 8-μm pore size). The cocultured strains were split into the upper and lower chambers. In total, 1 mL of BHI broth was added to the upper chamber and $1 \times 10^7$ of each strain was inoculated from ON cultures. Plates were covered with a lid and incubated for 24 h statically at 37 °C in microaerophilic conditions.

**Subcellular Fractionation.** The *Lm* fractionation was performed as described previously (20) with a few modifications. The cell-wall, membrane, and cytoplasm compartments were separated from 2 mL of stationary-phase culture ($OD_{600}$ 2). The bacteria were pelleted and filtered, and filtered supernatant was precipitated at −20 °C ON with 16% trichloroacetic acid (TCA). The bacterial pellet was washed once with 2 mL of PBS and once with 2 mL of TS buffer (10 mM Tris·HCl, pH 6.9, 10 mM MgCl₂, and 0.5 M sucrose). Then the bacteria were resuspended in 1 mL of TS buffer containing 45 μg mutanolysin (Sigma) and cOmplete protease inhibitor mixture (Roche) ON statically at 37 °C to digest completely the cell wall. Protoplasts were pelleted for 5 min at $15,000 \times g$ and the cell-wall fraction was precipitated with TCA as indicated before for the supernatant. The protoplasts were lysed by four freeze–thaw cycles (liquid nitrogen and a water bath at 37 °C) in 100 μL of protoplast buffer (100 mM Tris·HCl, pH 7.5, 100 mM NaCl, and 10 mM MgCl₂). The membrane and the cytoplasm fractions were centrifuged at 4 °C for 15 min at $16,000 \times g$. The pellet corresponding to the membrane fraction was then resuspended in 100 μL of 3-((3-cholamidopropyl) dimethylammonio)-1-propanesulfonate (CHAPS) lysis buffer (30 mM Tris·HCl, pH 7.5, 150 mM NaCl, and 1% CHAPS). The membrane fraction was sonicated (three cycles of 15 s, 20% amplitude).

Meza-Torres et al.
Listeriolysin S: A bacteriocin from *Listeria monocytogenes* that induces membrane permeabilization in a contact-dependent manner

PNAS | 9 of 11
https://doi.org/10.1073/pnas.2108155118

**Immunogold Labeling and Transmission Electron Microscopy.** Bacteria were grown in BHI broth ON and the cultures were refreshed until the bacteria reached an OD$_{600nm}$ of 2. Strain *Lm* F2365 pHELP: *llsA*-HA was used to detect LLS and the strain without the tag *Lm* F2365 pHELP: *llsA* was used as a negative control. Bacteria were fixed with 2% paraformaldehyde + 0.1% glutaraldehyde in PHEM buffer (60 mM Pipes, 25 mM Hepes, pH 7, 2 mM MgCl$_2$, and 10 mM ethylene glycol tetraacetic acid) for 2 h at room temperature. After fixation, bacteria were washed with PHEM buffer and the remaining free aldehydes were quenched with 50 mM NH$_4$Cl in PHEM buffer. Bacteria were pelleted down and embedded in 12% gelatin in PBS. After solidification on ice, the bacterial pellet was cut into small cubes of 1 mm$^3$. The cubes were incubated ON in 2.1 M sucrose in PBS and mounted afterward on metal pins for plunge freezing in liquid nitrogen. Cryosections with a nominal feed of 60 nm were cut with a Leica UC6/FC6 and picked up with a 1:1 mixture of 2.1 M sucrose in PBS and 2% methylcellulose in water. After thawing, the sections were deposited on 200-mesh copper grids coated with a formvar and carbon film. Immunolabeling according to the protein A gold method was done as described (48). The rabbit monoclonal antibody anti-HA (clone 3F10; Roche; 1:100 dilution) and the rat anti-rabbit conjugated antibody (Epitomics; 1:200) followed by protein A gold (10 nm; CMC Utrecht) were used. Images were taken with a Tecnai G2 microscope run at 120 kV, equipped with a Gatan US 4000.

**Superresolution Microscopy.** The superresolution microscopy (PAINT/dSTORM) experiments were done on a custom-built microscope as described before (49). The Nikon TiE Eclipse microscope body was equipped as described before (50). Briefly, the microscope was equipped with a 100× numerical aperture 1.49 oil immersion objective lens, an ultrasensitive electron-multiplying charge-coupled device (EM-CCD) camera (Andor iXon Ultra 888), and a couple of dual–band-pass dichroic mirrors, and the attached laser box is composed of four high-power lasers: a 405 nm–100 mW laser (Oxxius), a 488 nm–500 mW laser, a 561 nm–500 mW laser, and a 642 nm–500 mW laser (MPB Communications). The wavelength selection was done using an optoelectronic device (AA Opto Electronic). For detailed methods and analysis of images, see *SI Appendix, Materials and Methods*.

**Microfluidics and Time-Lapse Microscopy.** Time-lapse microscopy was performed with an inverted Delta Vision Elite microscope (GE Healthcare) equipped with a UPLFLN100XO2/PH3/1.30 objective (Olympus). An environmental chamber at 37 °C was used enclosing the optical components of the microscope, the polydimethylsiloxane (PDMS) device, and the stage (WeatherStation Precision Control; Applied Precision). Images were recorded with a personal Delta Vision system equipped with a high-speed sCMOS camera. The exposure time and illumination power settings were as follows: phase contrast: 150 ms at 50% transmission (T); DAPI (excitation [Ex]: 360/40; emission [Em]: 457/50): 100 ms at 32% T; fluorescein isothiocyanate (Ex: 475/28; Em: 525/48): 100 ms at 32% T; and mCherry (Ex: 575/25; Em: 632/60): 100 ms at 32% T. Images were recorded for 10 h at 15-min intervals for the SYTOX assays and at 8-min intervals for the growth rate assays. For the

time-lapse microscopy, a customized microfluidic device was used as described before with some modifications (25). For detailed methods and analysis of images, see *SI Appendix, Materials and Methods*.

**Membrane-Depolarization Assays and Fluorescence Microscopy.** Cocultures were prepared as indicated previously. The dye DiBAC$_4$(3) was added to the BHI medium (final concentration 2.5 μM) when the cocultures were prepared. Nisin was used as a positive control (final concentration 5 μM). After 3, 4, and 6 h of coculture, bacteria were washed once and resuspended in PBS, mounted on a glass coverslip with Fluoromount-G mounting medium (Interchim), and dried in the dark at 37 °C for 30 min. Slides were observed with an AxioObserver.Z1 inverted microscope (Carl Zeiss) equipped with a high-speed CSU-X1 spinning-disk confocal system (Yokogawa) and an Evolve EM-CCD camera (Photometrics). Images were acquired through a Plan-Apochromat 100× oil objective, using MetaMorph software (version 7.7.9.0). Stacks of 20 images were acquired every 200 nm in the z axis. Three-dimensional reconstruction was performed on stacks with IMARIS software (Bitplane; Oxford Instruments). Icy was used for image processing and analysis. For each condition tested, at least 150 cells were marked as regions of interest (ROIs) manually by using only one image of the Z stacks (better focused image). To quantify the effects of depolarization, ROI mean pixel intensities of the GFP channel were obtained and normalized to the background mean pixel intensities of the GFP channel.

**Statistics.** The Shapiro–Wilk test was used to test the normal distribution of datasets. Normally distributed data with equal group variances were expressed as means ± SEM. Statistical tests were performed using Prism 8.0 (GraphPad Software) and differences were evaluated by an unpaired Student's *t* test or unpaired multiple *t* tests as indicated. The level of significance was set at *$P < 0.05$. Significant differences are represented by asterisks (*$P < 0.05$, **$P < 0.01$, ***$P < 0.001$, ****$P < 0.0001$).

**Data Availability.** All study data are included in the article and/or *SI Appendix*.

1. P. Cossart, Illuminating the landscape of host-pathogen interactions with the bacterium *Listeria monocytogenes*. *Proc. Natl. Acad. Sci. U.S.A.* **108**, 19484–19491 (2011).

2. L. Radoshevich, P. Cossart, *Listeria monocytogenes*: Towards a complete picture of its physiology and pathogenesis. *Nat. Rev. Microbiol.* **16**, 32–46 (2018).

3. P. D. Cotter et al., Listeriolysin S, a novel peptide haemolysin associated with a subset of lineage I *Listeria monocytogenes*. *PLoS Pathog.* **4**, e1000144 (2008).

4. R. H. Orsi, H. C. den Bakker, M. Wiedmann, *Listeria monocytogenes* lineages: Genomics, evolution, ecology, and phenotypic characteristics. *Int. J. Med. Microbiol.* **301**, 79–96 (2011).

5. E. M. Clayton, C. Hill, P. D. Cotter, R. P. Ross, Real-time PCR assay to differentiate Listeriolysin S-positive and -negative strains of *Listeria monocytogenes*. *Appl. Environ. Microbiol.* **77**, 163–171 (2011).

6. J. J. Quereda et al., Listeriolysin S is a streptolysin S-like virulence factor that targets exclusively prokaryotic cells in vivo. *mBio* **8**, e00259-17 (2017).

7. J. J. Quereda et al., Bacteriocin from epidemic *Listeria* strains alters the host intestinal microbiota to favor infection. *Proc. Natl. Acad. Sci. U.S.A.* **113**, 5706–5711 (2016).

8. J. J. Quereda, J. Meza-Torres, P. Cossart, J. Pizarro-Cerdá, Listeriolysin S: A bacteriocin from epidemic *Listeria* strains that targets the gut microbiota. *Gut Microbes* **8**, 384–391 (2017).

9. S. W. Lee et al., Discovery of a widely distributed toxin biosynthetic gene cluster. *Proc. Natl. Acad. Sci. U.S.A.* **105**, 5879–5884 (2008).

10. E. M. Molloy, P. D. Cotter, C. Hill, D. A. Mitchell, R. P. Ross, Streptolysin S-like virulence factors: The continuing sagA. *Nat. Rev. Microbiol.* **9**, 670–681 (2011).

11. K. J. Molohon et al., Plantazolicin is an ultra-narrow spectrum antibiotic that targets the *Bacillus anthracis* membrane. *ACS Infect. Dis.* **2**, 207–220 (2016).

12. Y. M. Li, J. C. Milne, L. L. Madison, R. Kolter, C. T. Walsh, From peptide precursors to oxazole and thiazole-containing peptide antibiotics: Microcin B17 synthase. *Science* **274**, 1188–1193 (1996).

13. J. L. Vizán, C. Hernández-Chico, I. del Castillo, F. Moreno, The peptide antibiotic microcin B17 induces double-strand cleavage of DNA mediated by *E. coli* DNA gyrase. *EMBO J.* **10**, 467–476 (1991).

14. V. Datta et al., Mutational analysis of the group A streptococcal operon encoding streptolysin S and its virulence role in invasive infection. *Mol. Microbiol.* **56**, 681–695 (2005).

15. V. Nizet, Streptococcal beta-hemolysins: Genetics and role in disease pathogenesis. *Trends Microbiol.* **10**, 575–580 (2002).

16. A. W. Bernheimer, Disruption of wall-less bacteria by streptococcal and staphylococcal toxins. *J. Bacteriol.* **91**, 1677–1680 (1966).

17. H. Keiser, G. Weissmann, A. W. Bernheimer, Studies on lysosomes. IV. Solubilization of enzymes during mitochondrial swelling and disruption of lysosomes by streptolysin S and other hemolytic agents. *J. Cell Biol.* **22**, 101–113 (1964).

18. W. Hryniewicz, J. Pryjma, Effect of streptolysin S on human and mouse T and B lymphocytes. *Infect. Immun.* **16**, 730–733 (1977).

19. D. L. Higashi et al., Activation of band 3 mediates group A *Streptococcus* streptolysin S-based beta-haemolysis. *Nat. Microbiol.* **1**, 15004 (2016).

20. R. Jonquières, H. Bierne, F. Fiedler, P. Gounon, P. Cossart, Interaction between the protein InlB of *Listeria monocytogenes* and lipoteichoic acid: A novel mechanism of protein association at the surface of gram-positive bacteria. *Mol. Microbiol.* **34**, 902–914 (1999).

21. D. A. Mitchell et al., Structural and functional dissection of the heterocyclic peptide cytotoxin streptolysin S. *J. Biol. Chem.* **284**, 13004–13012 (2009).

22. C. K. Spahn et al., A toolbox for multiplexed super-resolution imaging of the E. coli nucleoid and membrane using novel PAINT labels. Sci. Rep. 8, 14768 (2018).

23. A. Sharonov, R. M. Hochstrasser, Wide-field subdiffraction imaging by accumulated binding of diffusing probes. Proc. Natl. Acad. Sci. U.S.A. 103, 18911–18916 (2006).

24. S. van de Linde et al., Direct stochastic optical reconstruction microscopy with standard fluorescent probes. Nat. Protoc. 6, 991–1009 (2011).

25. G. Manina, A. Griego, L. K. Singh, J. D. McKinney, N. Dhar, Preexisting variation in DNA damage response predicts the fate of single mycobacteria under stress. EMBO J. 38, e101876 (2019).

26. D. Balestrino et al., Single-cell techniques using chromosomally tagged fluorescent bacteria to study Listeria monocytogenes infection processes. Appl. Environ. Microbiol. 76, 3625–3636 (2010).

27. H. Lee, E.-R. Woo, D. G. Lee, Glochidioboside kills pathogenic bacteria by membrane perturbation. Curr. Microbiol. 71, 1–7 (2015).

28. R. Bauer, L. M. T. Dicks, Mode of action of lipid II-targeting lantibiotics. Int. J. Food Microbiol. 101, 201–216 (2005).

29. J. D. Te Winkel, D. A. Gray, K. H. Seistrup, L. W. Hamoen, H. Strahl, Analysis of antimicrobial-triggered membrane depolarization using voltage sensitive dyes. Front. Cell Dev. Biol. 4, 29 (2016).

30. J.-D. Sauer, A. A. Herskovits, M. X. D. O'Riordan, Metabolism of the gram-positive bacterial pathogen Listeria monocytogenes. Microbiol. Spectr. 7, GPP3-0066-2019 (2019).

31. P. Chandrangsu, R. Dusi, C. J. Hamilton, J. D. Helmann, Methylglyoxal resistance in Bacillus subtilis: Contributions of bacillithiol-dependent and independent pathways. Mol. Microbiol. 91, 706–715 (2014).

32. O. Davies, P. Mendes, K. Smallbone, N. Malys, Characterisation of multiple substrate-specific (d)ITP/(d)XTPase and modelling of deaminated purine nucleotide metabolism. BMB Rep. 45, 259–264 (2012).

33. S. B. Gabelli, M. A. Bianchet, M. J. Bessman, L. M. Amzel, The structure of ADP-ribose pyrophosphatase reveals the structural basis for the versatility of the Nudix family. Nat. Struct. Biol. 8, 467–472 (2001).

34. C. Harrison, GrpE, a nucleotide exchange factor for DnaK. Cell Stress Chaperones 8, 218–224 (2003).

35. R. Gutknecht, R. Beutler, L. F. Garcia-Alles, U. Baumann, B. Erni, The dihydroxyacetone kinase of Escherichia coli utilizes a phosphoprotein instead of ATP as phosphoryl donor. EMBO J. 20, 2480–2486 (2001).

36. C. Loridan, J. E. Alouf, Purification of RNA-core induced streptolysin S, and isolation and haemolytic characteristics of the carrier-free toxin. J. Gen. Microbiol. 132, 307–315 (1986).

37. T. S. Theodore, G. B. Calandra, Streptolysin S activation by lipoteichoic acid. Infect. Immun. 33, 326–328 (1981).

38. R. Saar-Dover et al., D-alanylation of lipoteichoic acids confers resistance to cationic peptides in group B Streptococcus by increasing the cell wall density. PLoS Pathog. 8, e1002891 (2012).

39. E. Abachin et al., Formation of D-alanyl-lipoteichoic acid is required for adhesion and virulence of Listeria monocytogenes. Mol. Microbiol. 43, 1–14 (2002).

40. B. M. Xavier, A. J. Houlihan, J. B. Russell, The activity and stability of cell-associated activity of bovicin HC5, a bacteriocin from Streptococcus bovis HC5. FEMS Microbiol. Lett. 283, 162–166 (2008).

41. A. Barbour, K. Philip, Variable characteristics of bacteriocin-producing Streptococcus salivarius strains isolated from Malaysian subjects. PLoS One 9, e100541 (2014).

42. H. Daba, C. Lacroix, J. Huang, R. E. Simard, L. Lemieux, Simple method of purification and sequencing of a bacteriocin produced by Pediococcus acidilactici UL5. J. Appl. Bacteriol. 77, 682–688 (1994).

43. I. Wiedemann et al., Specific binding of nisin to the peptidoglycan precursor lipid II combines pore formation and inhibition of cell wall biosynthesis for potent antibiotic activity. J. Biol. Chem. 276, 1772–1779 (2001).

44. D. J. Gonzalez et al., Clostridiolysin S, a post-translationally modified biotoxin from Clostridium botulinum. J. Biol. Chem. 285, 28220–28228 (2010).

45. L. García-Bayona, M. S. Guo, M. T. Laub, Contact-dependent killing by Caulobacter crescentus via cell surface-associated, glycine zipper proteins. eLife 6, e24869 (2017).

46. J. C. Whitney et al., A broadly distributed toxin family mediates contact-dependent antagonism between gram-positive bacteria. eLife 6, e26938 (2017).

47. L. McNally et al., Killing by type VI secretion drives genetic phase separation and correlates with increased cooperation. Nat. Commun. 8, 14371 (2017).

48. J. W. Slot, H. J. Geuze, S. Gigengack, G. E. Lienhard, D. E. James, Immuno-localization of the insulin regulatable glucose transporter in brown adipose tissue of the rat. J. Cell Biol. 113, 123–135 (1991).

49. M. Lelek et al., Superresolution imaging of HIV in infected cells with FlAsH-PALM. Proc. Natl. Acad. Sci. U.S.A. 109, 8564–8569 (2012).

50. V. Rincheval et al., Functional organization of cytoplasmic inclusion bodies in cells infected by respiratory syncytial virus. Nat. Commun. 8, 563 (2017).

**MICROBIOLOGY**

Meza-Torres et al.
Listeriolysin S: A bacteriocin from Listeria monocytogenes that induces membrane permeabilization in a contact-dependent manner

PNAS | 11 of 11
https://doi.org/10.1073/pnas.2108155118